2011

The cool ZZ Ceti star PG 2303+243: observations and analysis of variability in 2004

E. Pakstiene

J. E. Solheim

G. Handler

Michael D. Reed
Missouri State University

Zs Bognar

See next page for additional authors

Recommended Citation

Pakštienė, E., J-E. Solheim, G. Handler, M. Reed, Zs Bognár, F. Rodler, M. Paparó, J. Zdanavičius, B. Steininger, and G. Wolf. "The cool ZZ Ceti star PG 2303+ 243: observations and analysis of variability in 2004." Monthly Notices of the Royal Astronomical Society 415, no. 2 (2011): 1322-1333.

Monthly Notices
of the
ROYAL ASTRONOMICAL SOCIETY

Mon. Not. R. Astron. Soc. **415,** 1322–1333 (2011) doi:10.1111/j.1365-2966.2011.18781.x

The cool ZZ Ceti star PG 2303+243: observations and analysis of variability in 2004

E. Pakštienė,[1⋆] J.-E. Solheim,[2] G. Handler,[3] M. Reed,[4] Zs. Bognár,[5] F. Rodler,[3,6] M. Paparó,[5] J. Zdanavičius,[1] B. Steininger[3] and G. Wolf[4]

[1]*Institute of Theoretical Physics and Astronomy, Vilnius University, Goštauto 12, Vilnius LT-01108, Lithuania*
[2]*Institute of Theoretical Astrophysics, University of Oslo, PO Box 1029, Blindern, NO 0315 Oslo, Norway*
[3]*Institut für Astronomie, Universität Wien, Türkenschanzstrasse 17, A-1180 Wien, Austria*
[4]*Baker Observatory, Missouri State University, Springfield, MO 65648, USA*
[5]*Konkoly Observatory, Hungarian Academy of Sciences, PO Box 67, Konkoly Thege út 15-17, H-1525 Budapest, Hungary*
[6]*Instituto de Astrofísica de Canarias, C/Vía Láctea s/n, E-38205 La Laguna, Tenerife, Spain*

Accepted 2011 March 23. Received 2011 March 23; in original form 2010 June 8

ABSTRACT

PG 2303+243 is a cool DA variable (also called ZZ Ceti) star with a rich pulsation spectrum and variable amplitudes. A mini-campaign involving six observatories yielded time-resolved photometric measurements of PG 2303+243 during the period 2004 September 5–20. A duty cycle of 35 per cent was achieved. We detected 24 possible independent frequencies, their amplitudes and phases for future mode identification. We confirm the occurrence of short-term amplitude and frequency variations. Our analysis suggests an $l = 1$ rotational splitting around 8.4 μHz, implying a rotation period of 16.5 h.

Key words: stars: individual: PG 2303+243 – stars: variables: general – white dwarfs.

1 INTRODUCTION

White dwarf (WD) stars are the final evolutionary stage of ∼97 per cent of all stellar objects (e.g. Weidemann 2000; Pech, Vauclair & Dolez 2006). Whereas optical and ultraviolet spectroscopy and detailed modelling have resulted in significant progress in understanding the atmospheres, compositions and evolution of WDs, the interior structures of stars can be deduced in detail by reproducing oscillation spectra of pulsators with theoretical models. This method is called asteroseismology.

Most WDs do not pulsate, but in some limited regions along their cooling sequence, pulsators can be found (e.g. Winget 1988). WDs of spectral type DA, dominated by hydrogen lines, represent ∼80 per cent of the total WD population (Fleming, Liebert & Green 1986; De Gennaro et al. 2008). This provides additional impetus to determine their internal structure as accurately as possible (Bradley 1998; Pech et al. 2006; Castanheira & Kepler 2009).

Pulsating WDs, on the other hand, are rather short-lived phases in the evolution of these objects. Their internal structures can be assumed to be the same as that of non-pulsators because most, if not all, DA WDs do pulsate as they pass through the instability strip (Gianninas, Bergeron & Fontaine 2006). The pulsations are due to non-radial gravity (g) modes and rich oscillation spectra may be used to deduce their global properties, such as mass, rotation period and magnetic field, and to derive convection properties (Fontaine & Brassard 2008; Winget & Kepler 2008; Althaus et al. 2010). Structural information about their outer layers can also be obtained, including the depth of the hydrogen and/or helium envelope (Castanheira & Kepler 2008) and the size of compositional transition zones (H/He, He/C) (Bischoff-Kim, Montgomery & Winget 2008a).

Studies of pulsating WD stars have already yielded spectacular results and have opened new windows for understanding the structure of WDs in general. Asteroseismology is now extending beyond the traditionally conceived boundaries of matching models to observed oscillation frequencies: many recent investigations of pulsating WDs attempt to determine physical properties of the surface convection zone. Initially suggested by Brickhill (1983), methods for constraining convection were further developed by Montgomery (2005a,b, 2007).

The determination of the cooling rate of the WD G 117-B15A from precise pulsational period change measurements (Kepler et al. 2005b) made it even possible to obtain strong upper limits for the axion mass (Córsico et al. 2001). This may be improved by studies of other WD stars (Bischoff-Kim et al. 2008a; Bischoff-Kim, Montgomery & Winget 2008b). In this manner, many useful results have already been born of WD asteroseismology, and we anticipate more will be forthcoming.

1.1 ZZ Ceti stars

DA variables (DAVs) are also known as ZZ Ceti stars after the prototype of the class (ZZ Ceti = Ross 548). They constitute the

⋆E-mail: erika.pakstiene@tfai.vu.lt

most numerous class of pulsating WDs with about 150 known members (Castanheira et al. 2010). A systematic study of ZZ Ceti pulsators was first undertaken by pioneers in the field such as Robinson (1980), McGraw et al. (1981) and Winget & Fontaine (1982). Clemens (1993) was the first to demonstrate systematically the distinct behaviour of pulsation periods and amplitudes as a function of temperature for a significant sample of DAVs. The full sample of 80 ZZ Ceti stars that were known at the time was used for an investigation of the pulsation properties of DAVs across the instability strip, showing that the cool DAVs (cDAVs) on average have more modes excited to visible amplitude than the hot ones (Mukadam et al. 2006).

1.2 The instability strip of ZZ Ceti stars

Hydrogen atmosphere non-interacting DA WDs are observed to pulsate in an instability strip located in the temperature range of 10 800–12 500 K for $\log g = 8$ (Bergeron et al. 1995; Koester & Allard 2000; Koester & Holberg 2001; Bergeron et al. 2004; Mukadam et al. 2004; Gianninas et al. 2006; Mukadam et al. 2006; Castanheira et al. 2007). The instability strip for accreting pulsating WDs is wider and ranges from 10 500 to 15 000 K (Szkody et al. 2010). Recent studies have determined that the width of the DA instability strip for non-interacting WDs is only about 1000–1200 K in temperature and spans about 1300 s in period (Mukadam et al. 2004; Gianninas, Bergeron & Fontaine 2005). The internal uncertainty in measuring temperatures of DA WDs using spectra is typically about 200 K, which is 17–20 per cent of the width of the instability strip. The masses of ZZ Ceti stars lie between 1.1 $M_\odot$ (Kanaan et al. 1998) and 0.5 $M_\odot$ (Kepler et al. 2006). The ZZ Ceti instability strip appears trapezoidal in the Hertzsprung–Russell (HR) diagram because of the dependence of its blue and red boundaries on stellar mass. The time-scale for crossing the instability strip is almost 1 Gyr (e.g. Castanheira et al. 2007).

From the sample of DA WDs from the Sloan Digital Sky Survey (SDSS), Mukadam et al. (2004) concluded that non-pulsating stars coexist with pulsating stars at the same location in the instability strip. However, the SDSS non-pulsators are faint, and therefore the spectra used to determine their atmospheric parameters have poor signal-to-noise ratio (Kleinman et al. 2004). This increases the uncertainty in the locations of these stars in the HR diagram (Pech et al. 2006). In addition, these so-called not-observed-to-vary (NOV) stars can in fact be low-amplitude pulsators (Castanheira et al. 2007, 2010), which would provide strong observational evidence for a pure ZZ Ceti instability strip. We may therefore assume that all WDs evolving through the pulsation band will pulsate and that the properties deduced from pulsations of the ZZ Ceti stars are valid for all DA WDs as a group.

1.3 Classification of ZZ Ceti stars

ZZ Ceti stars are usually divided into hot DAVs (hDAVs) and cDAVs. The hot ZZ Ceti stars are recognized as simple pulsators that exhibit a few modes with short periods (200–300 s), have small amplitudes [few mili-modulation-amplitude (mma)], sinusoidal or saw-tooth pulse shapes, and continue to show stable pulsation spectra over a few decades. The cool ZZ Ceti stars are complex pulsators that exhibit several long periods (600–1200 s) with large amplitudes (40–110 mma), non-sinusoidal pulse shapes with fast rise times and slowly decaying brightness, and with an amplitude modulation over time-scales of a few days to a few years.

However, a clear dividing point (in temperature) between these two types does not exist, because the location and width of the instability strip are extremely difficult to determine empirically. Very small errors in the reduction of observed spectra or minor differences in the theoretical treatment of convection can cause differences up to 2000 K in the derived effective temperatures (Bergeron et al. 1995; Koester & Vauclair 1997; Koester & Allard 2000; Koester et al. 2009; Tremblay & Bergeron 2009).

Mukadam et al. (2006) have suggested a new ZZ Ceti classification scheme based on the weighted mean period (WMP) as a temperature indicator of these variables. Mukadam et al. (2006) have redefined the class of hDAVs as ZZ Ceti stars with WMP < 350 s, the class of cDAVs as ZZ Ceti stars with WMP > 650 s, and suggested introducing a new class of DAVs, to be called the intermediate DAVs (iDAVs), as ZZ Ceti stars with $350 <$ WMP < 650 s. The iDAVs form the evolutionary subclass adjoining the hot and cool ZZ Ceti stars and typically encompass ZZ Ceti pulsators that show a large range of pulsation periods. The qualitative explanation for the change in pulsation spectra within the ZZ Ceti instability strip is based on the behaviour of the convection zone (see Section 1.5).

1.4 What can we learn from ZZ Ceti stars?

As WDs are the last evolutionary stage of low- and intermediate-mass stars, which form the vast majority of all stars, it is important to know their internal structure as precisely as possible. Calibration of the WD cooling sequence could potentially be used as a cosmological tool for age determination independent from other methods (Winget et al. 1987; Dolez et al. 2006). However, this goal is not yet realized due to uncertainties in the models (Fontaine, Brassard & Bergeron 2001; Winget & Kepler 2008).

Asteroseismic studies of ZZ Ceti stars can help to reduce some of these uncertainties by constraining the stars' total masses and hydrogen mass fractions (Dolez et al. 2006). Asteroseismology is a powerful tool to infer precisely the internal structure of variable stars. Knowing the interior structure of DA WDs is important in many respects and justifies continuous efforts to derive it from asteroseismology. By comparing observed periods of oscillation with periods predicted by non-radial pulsation theory, it is possible to derive the structure of the model that best represents the observations (Pech et al. 2006).

The study of ZZ Ceti stars and their seismology is beneficial when striving to understand the structure of WDs in general as they are otherwise normal DA WDs (Bradley 1998). Multisite campaigns, such as those carried out by the Whole Earth Telescope (WET; Nather et al. 1990), have enabled us to explore the interior structure of one of the hottest DAV stars, G117-B15A (RY LMi or WD 0921+354; Kepler et al. 1995), via asteroseismology. However, as the hotter DAV stars tend to have only a few short-period modes, such investigations are difficult because many models can fit the observations, and the small number of observed modes implies fewer constraints on the stellar structure (Bradley 1998). Although the pulsation amplitudes become increasingly variable as the ZZ Ceti stars approach the red edge of the instability strip, the cooler DAV stars have more independent pulsation modes excited and are therefore potentially richer targets for asteroseismology.

1.5 Convection within cool ZZ Ceti stars

Two different mechanisms (convection and the $\kappa - \gamma$ mechanism) are responsible for exciting pulsations in ZZ Ceti stars. The κ-mechanism due to partial ionization is closely linked to the action of diffusive processes, which determine the local contents of heavy

elements in the stellar envelope. Whatever the driving mechanism, it is essential that the pulsation periods be of the order of the thermal time-scale of the driving zone. In the $\kappa - \gamma$ mechanism, driving occurs locally when the opacity varies so that a net amount of radiative flux is still flowing into a region at maximum compression (Montgomery et al. 2008). Close to the blue edge of the instability strip, the fraction of the flux transported by convection is negligible. Here the $\kappa - \gamma$ mechanism, due to the partial ionization of hydrogen, is responsible for the instability (Dolez & Vauclair 1981; Winget et al. 1982; Dolez et al. 2006).

As WDs cool within the instability strip, the convection zone becomes larger when the star progresses to the red edge of the instability strip, allowing more modes to be excited. Convection starts at the base of the partial ionization layer which moves inwards as the star cools. The hydrogen mass fraction of DA WDs can be determined by an examination of the convection process in cool ZZ Ceti stars. In these cool ZZ Ceti stars, the excited periods are rather long because the base of the convection zone is deeper and the thermal time-scale is longer. In addition, more energy is required to heat the upper layers in cooler stars, which leads to higher pulsation amplitudes. The oscillation modes in cool ZZ Ceti stars are driven by convection, which causes several effects. Overall, they have more pulsation energy, the power spectra become more complex, the amplitudes can vary dramatically (even during one night), non-sinusoidal pulse shapes are observed and combination frequencies can be detected (Vuille & Brassard 2000; Wu 2001; Handler, Romero-Colmenero & Montgomery 2002; Yeates et al. 2005; Dolez et al. 2006). The depth of the convection zone varies and non-linearities occur within the surface flux perturbations. At the red edge of the instability strip, almost all the flux is carried by convection, and many modes are damped, with fewer available for asteroseismology (Dolez et al. 2006). Models cannot yet explain how the pulsations stop. All pulsation models predict a much cooler red edge than is observed. Wu & Goldreich (2001) suspect that excited modes may be discovered below the red edge by detection of their photospheric velocity variations.

The ZZ Ceti stars close to the red edge of the instability strip can be very useful for asteroseismology. A large number of modes and their dependence on interior structure and convection parameters help in finding the best stellar model and the location of the red edge. For that purpose, we have chosen to observe the cool ZZ Ceti star PG 2303+243. In this paper, we describe the observations of PG 2303+243 during a mini-campaign in 2004. We present light curves (LCs) and their Fourier transformations (FTs), observed frequencies with their amplitudes and phases, and discuss a list of possible independent frequencies.

1.6 PG 2303+243

Among the cooler DAV (ZZ Ceti) WDs, the light variations of PG 2303+243 were discovered to exhibit a rich Fourier spectrum (Vauclair, Dolez & Chevreton 1987). The star was classified by Mukadam et al. (2006) as a cDAV with $T_{\rm eff} = 11\,480$ K, $\log g = 8.09$ and independent modes with periods/amplitudes of 900.5 s/16 mma, 794.5 s/56 mma, 675.4 s/8 mma, 623.4 s/15 mma and 570.7 s/8 mma. The large amplitudes and number of frequencies made PG 2303+243 a good candidate for asteroseismic studies.

The improved time resolution (4 μHz) of a data set from 1990 (Vauclair et al. 1992) allowed the detection of as many as 22 periods for PG 2303+243. In spite of large amplitude variations, the period distribution seemed to have remained the same during the 4-yr interval from 1986 to 1990. The latter observations of PG 2303+243 were carried out as an observing campaign between the Steward Observatory's Mt Lemmon 1.5-m telescope and the 2.5-m Nordic Optical Telescope in 1990 October. Those five runs totalled $\simeq$27 h and revealed the presence of many modes; 22 independent mode frequencies were suggested. Drastic variations in amplitude over a short time-scale (<10 d) were observed.

After eliminating alias frequencies, a total of 11 combination signals were found. These frequencies could either occur by chance due to the richness of the g-mode spectrum and would have no other physical meaning, or they could be the result of non-linear superposition of modes and would then indicate the presence of non-linear mode coupling (Brassard et al. 1992).

Vauclair et al. (1992) attempted a preliminary identification of the modes observed in PG 2303+243, mainly based on period and trapping coefficient ratios. In this case, the observations constrained the thickness of the outer hydrogen layer to be in the range $-8.7 < \log Q(\mathrm{H}) < -7.6$, where $\log Q(\mathrm{H}) = \log (M_{\rm H}/M_*)$. Asteroseismology indicates $\log Q(\mathrm{H})$ for ZZ Ceti stars between -4 and -9.5 (Bradley 2001; Castanheira & Kepler 2009) with an average of -6.3 (Castanheira & Kepler 2009). The observations by Vauclair et al. (1992) suggest that the surface hydrogen layer of PG 2303+243 is thin rather than thick.

Observations of PG 2303+243 can help test the theory of convective driving (Brickhill 1992) as the convective turnover time-scale in DAs and DBs is much shorter than the pulsation period and as the depth of the convection zone varies during the pulsation period. This distorts the shape of the LC at the photosphere and creates combination frequencies and harmonics in the Fourier power spectrum.

2 OBSERVATIONS

Since PG 2303+243 had not been observed since 1992, and its pulsation spectrum changed from night to night, we decided to organize a mini-campaign to attempt to resolve it. We expected more than 22 periodicities to be present. A more robust determination of pulsation periods requires a data set of longer duration with a higher duty cycle than before. In addition, we planned to check the stability of the pulsation spectrum over time.

The PG 2303+243 mini-campaign was scheduled for 2004 September 5–20, with six observatories participating (see Table 1). We attempted to minimize bandpass issues by using CCDs with standard V filters to facilitate the combination of data from different sites. At the Molėtai Observatory, no filter was used because the wavelength response of the camera was sufficiently close to V.

Unfortunately, not all of the participants were able to acquire data. Lulin Observatory suffered a period of storms and consequently had no clear nights, but all the other observatories contributed data (see Table 2).

The raw data have been reduced according to the standard procedure used for WET observations. We used XQED for data reduction (Riddle 2003), which allows us to remove 'bad points' from observed data, subtract the sky background, make extinction corrections, divide the measurements of the target by those of the comparison star (if needed) and obtain individual LCs of PG 2303+243 for further analyses. The times of observations were transferred from UTC to the Barycentric Julian Ephemeris Date (BJED).

Different cycle times did not produce problems for FT calculations because we used the program PERIOD04 (Lenz & Breger 2005), which calculates Fourier spectra of unequally spaced data. Some representative LCs from different observatories are shown in Fig. 1,

Table 1. Participants of the PG 2303+243 mini-campaign during 2004 September 5–20.

Country	Observatory	Diameter of telescope	Latitude Longitude	Altitude	Observer(s)
Austria	University of Vienna Obs.	80 cm	+48.2316667 E16.336667	214 m	Gerald Handler, Florian Rodler Bruno Steininger
Hungary	Piszkestetö Obs.	100 cm	+47:55:08 E19:53:54	964 m	Margit Paparó Zsófia Bognár
Lithuania	Molėtai AO	31/51 cm, Maksutov	+55:18:57.5 E25:33:48.0	200 m	Justas Zdanavičius
Taiwan	Lulin Obs.	100 cm	+23:28:07 E120:52:25	2862 m	Chin-Wei Chen Wen-Shan Hsiao
USA, Missouri State	Baker Obs.	40 cm	+37:23:55.05 E266:57:29.7	418 m	Mike Reed, George Wolf Robert Patterson
Spain	Teide Obs.	80 cm	+28:18:00 E343:29:25	2400 m	Erika Pakštienė

Table 2. Observations of PG 2303+243. The detection limit is determined by a FAP of 0.001 (see Section 3.1.). Total resolution of the combined data is 0.76 μHz.

Instruments	Run name	Date (UT)	Start time (UT)	Run length (s)	No. of observed points	Cycle time (s)	Resolution (μHz)	Detection limit (mma)
Vienna 0.8	V5	05/09/2004	19:25:08	19 363	903	21	51.6	6.2
Vienna 0.8	V6	06/09/2004	18:20:08	32 060	1494	21	31.2	4.2
Vienna 0.8	V7	07/09/2004	19:58:04	14 889	667	21	67.2	5.8
Vienna 0.8	V8	08/09/2004	18:55:09	6715	320	21	148.9	9.8
Vienna 0.8	V9	09/09/2004	18:17:00	30 611	1468	21	32.7	5.6
Vienna 0.8	V10	10/09/2004	18:12:20	31 936	1450	21	31.3	3.5
Piszkestetö 1.0	K10	10/09/2004	18:44:43.8	25 462.5	962	23	39.3	3.1
Piszkestetö 1.0	K11	11/09/2004	19:18:52.7	16 070.6	225	63	62.2	4.8
Baker 0.4	B11	11/09/2004	04:40:01	22 265	634	31	44.9	4.0
Baker 0.4	B12	12/09/2004	03:50:54	25 453	638	31	39.3	3.8
Teide 0.8	T12	12/09/2004	21:52:00	28 890	1443	20	34.6	7.7
Vienna 0.8	V13_1	13/09/2004	19:10:18	10 286	451	21	97.2	4.8
Vienna 0.8	V13_2	13/09/2004	22:06:54	7056	341	21	141.7	
Teide 0.8	T13	13/09/2004	21:05:00	31 470	1558	20	31.8	5.7
Vienna 0.8	V14	14/09/2004	18:02:38	7884	376	21	126.8	11.1
Teide 0.8	T14	14/09/2004	20:01:00	34 670	1728	20	28.8	4.4
Teide 0.8	T15	15/09/2004	21:37:20	28 470	1423	20	35.1	4.9
Vienna 0.8	V16	16/09/2004	18:16:43	14 203	472	21	70.4	7.6
Teide 0.8	T16	16/09/2004	20:07:40	34 150	1705	20	29.3	4.9
Vienna 0.8	V17	17/09/2004	17:49:57	26 860	1292	21	37.2	4.6
Vienna 0.8	V19	19/09/2004	20:22:24	17 305	304	21	57.8	12.4
Molėtai 0.31/0.51	M19	19/09/2004	21:13:39	7642	188	39.2	130.9	7.6
Molėtai 0.31/0.51	M20	20/09/2004	18:30:03	18 119	450	39.2	55.2	7.6

and the combined LC from all measurements is shown in Fig. 2. The duty cycle of the final combined data set was 35.2 per cent.

3 ANALYSIS OF LIGHT CURVES AND FOURIER SPECTRA FROM SEPARATE RUNS

Fourier spectra of the reduced LCs shown in Fig. 2 were calculated with PERIOD04 (Lenz & Breger 2005). To determine all the pulsation frequencies in the star we used a pre-whitening procedure, i.e. peaks above a given significance level are removed one by one from the LC, starting with the most significant. At each stage of the search, a fit with the selected frequency was computed and subtracted from the data before a subsequent frequency search was started. The values of frequency, amplitude and phase were derived at each stage of pre-whitening and improved by fitting the original data with all the frequencies found up to then. The residuals after subtracting these sinusoids is called the pre-whitened LC, which can be pre-whitened as often as required to find significant frequencies in the Fourier spectrum. Comparing Fourier spectra from different runs, we found that most of the frequencies have unstable amplitudes, which sometimes changed dramatically from night to night, partially caused by beating.

Fig. 1 shows some of the PG 2303+243 LCs and Fourier spectra from different nights. The largest variations of amplitude in the Fourier spectrum occur at frequencies between 1027 and 1036 μHz: on 2004 September 09, the amplitude at these frequencies was around 42 mma; the next night it was only 10 mma and the third night almost 38 mma. Amplitudes at other frequencies changed as well, but less dramatically. The most stable amplitude is exhibited by a signal at a frequency of 1622 μHz (around 30 mma). Such changes of amplitude are common for cooler ZZ Ceti stars and warrant further investigations.

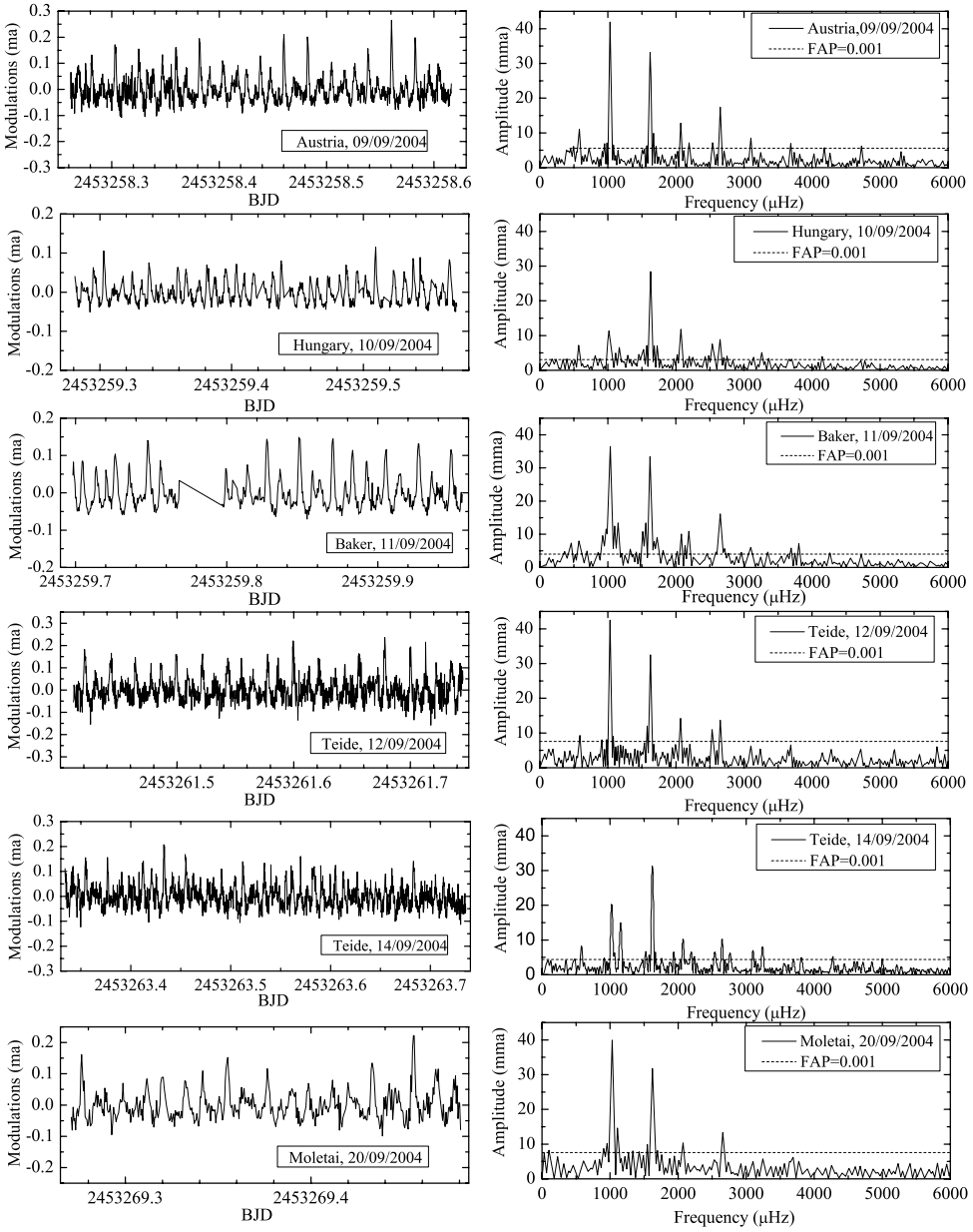

Figure 1. Example LCs and Fourier spectra [with a detection limit for false alarm probability (FAP) equal to 0.001] from different observatories during the mini-campaign of 2004 September 5–20.

3.1 Limit of detection

We need to determine a detection threshold to establish whether or not a periodicity is statistically significant. The false alarm probability (FAP) is the probability that one noise peak in N_i independent samples is above $P_{obs}/\langle P\rangle$ (Scargle 1982; Kepler 1993):

$$\mathrm{FAP} \cong N_i e^{-P_{obs}/\langle P\rangle} \quad (1)$$

or

$$P_{obs} = \ln\left(\frac{N_i}{\mathrm{FAP}}\right)\langle P\rangle, \quad (2)$$

where $\langle P\rangle$ is the average power in the frequency range under consideration, and P_{obs} corresponds to a detection limit in power ($P = A^2$, where A is the amplitude of the signal).

Therefore, if we have 10 000 independent samples, N_i, and only consider a peak real if it has a probability of less than 1 on 1000 to be due to noise (FAP = 1/1000), then $P_{obs} = 16.1\langle P\rangle$. That is, the peak must be 16.1 times taller than the average power to have one chance in 1000 to be due to noise only.

As the noise in the Fourier spectrum of combined LC depends on frequency, we did not adopt a constant detection limit over the whole frequency domain. We evaluated the frequency dependence of the detection limit on frequency using windows in the Fourier spectrum that contained no signal because the pulsation frequencies of PG 2303+243 increase the mean level of the Fourier spectrum. We tested linear and polynomial fits that gave similar results. For simplicity, we adopted a linear expression for the dependence of the detection limit on frequency ($A_{min} = 2.152\,75 - 1.181\,66 \times 10^{-4} \times f$).

For separate runs, we calculated and present only mean detection limits calculated using the same signal-free windows in the Fourier spectrum. The mean detection limits for each run are listed in the

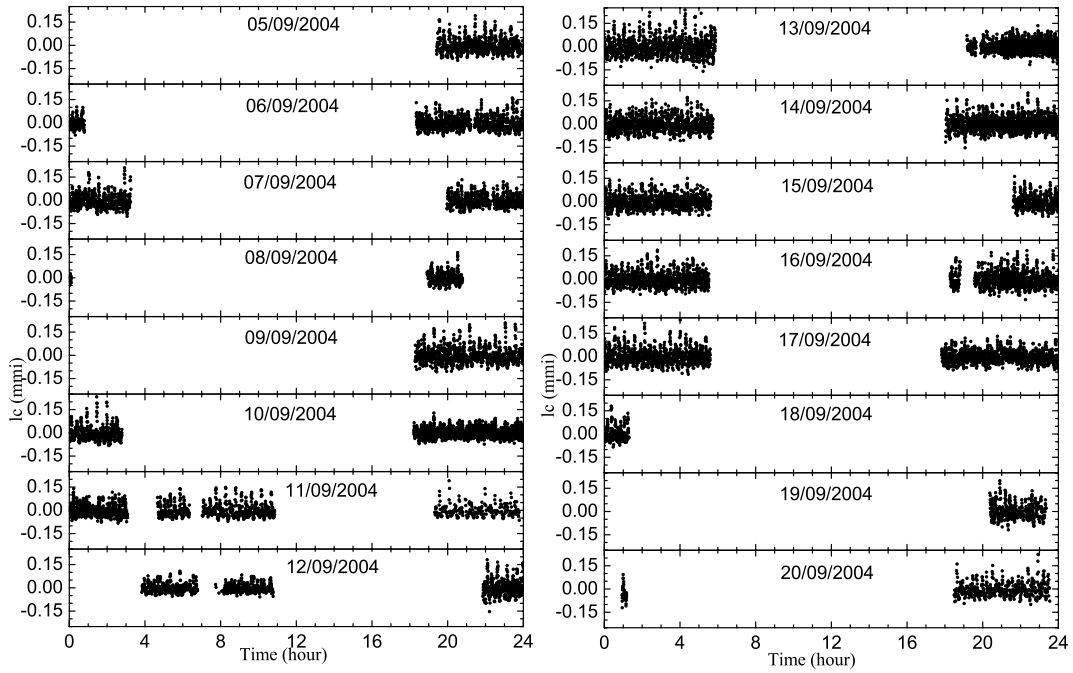

Figure 2. LCs from different observatories during the mini-campaign of 2004 September 5–20.

last column of Table 2 and plotted for some runs in Fig. 1. They not only give a measure of the quality of the data sets, but also change from run to run due to differing run lengths and because some peaks may appear and disappear in the frequency interval used for calculating the detection limit. In several cases, the detection limit was increased due to poor observing conditions. Some parts of the LCs that were strongly affected by clouds were not used in the analysis.

The detection limits for individual runs (see Table 2) vary between 3.1 and 12.4 mma. The lowest detection limit of 3.1 mma corresponds to the Piszkestetö data from 2004 September 10 under excellent weather conditions. In the same night, the detection limit in Vienna data was a bit larger (3.5 mma). This is understandable because the telescope at Piszkestetö (the largest telescope of the campaign) is located about 964 m above sea level at a mountain station and is larger than the Vienna telescope that is located in the city. The poorest detection limit of 12.4 mma corresponds to the worst observing conditions at the Vienna Observatory on 2004 September 09. However, the second highest detection limit of 11.1 mma does not indicate bad data quality; it is due to the short duration (7884 s) of the run. The detection limit becomes much smaller for combined LCs. The mean detection limit for the whole data set is 1.8 mma for FAP = 0.001.

Column 7 of Table 2 provides the cycle times for each run. Optimal cycle times, in terms of the lowest detection limit, were chosen by counterbalancing the high duty cycle (i.e. integration times which are long compared to readout times) of the observations with the effect of 'phase smearing'. This is caused by averaging the light variations over the integration time, which results in an undesirable apparent reduction of the pulsation amplitudes.

3.2 Analysis of individual runs

Using the pre-whitening procedure with PERIOD04, and the determined detection limits for amplitudes, we have determined the pulsation frequencies, amplitudes and phases for each run. The fitted

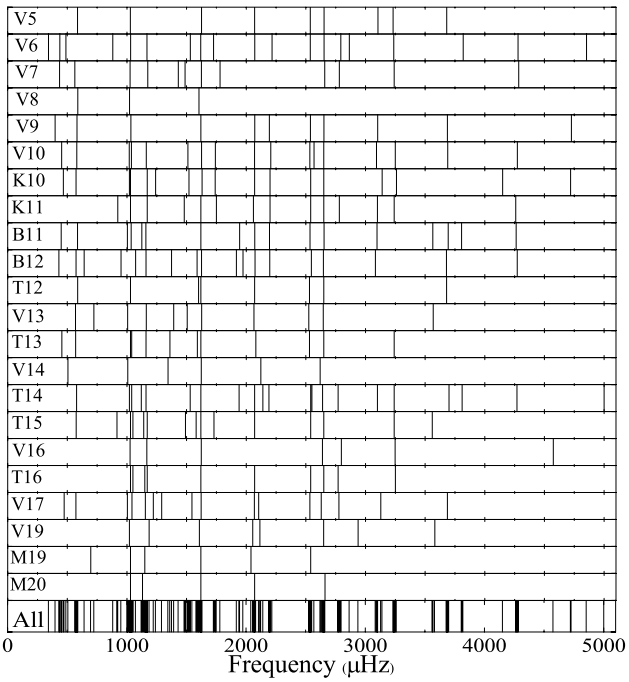

Figure 3. Schematic of detected frequencies of oscillations in PG 2303+243 for different observing runs during the mini-campaign of 2004 September 5–20. The bottom panel marked 'All' is a summation of the other panels.

frequencies are shown as a bar chart, in Fig. 3, which shows how frequencies change from run to run, with some of them disappearing and reappearing on subsequent runs. Most of these likely correspond to intrinsic pulsation frequencies of the star, and it is also possible that some of the pulsation frequencies themselves are changing slightly from run to run and may be even during the night. This is especially true for the small-amplitude pulsations where the

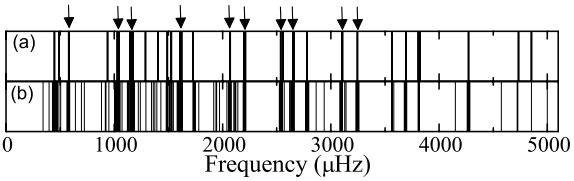

Figure 4. Schematic comparison of frequencies detected for (a) the combined LC with (b) those detected in individual runs. The arrows mark the frequencies detected most often (during more than 40 per cent of the observed runs).

bottom summary panel of Fig. 3 shows small clusters of bars. The Fourier peaks of some frequencies can become broadened because their amplitudes changed even during one night. PERIOD04 recognizes a broadened peak as a group of several narrow peaks at close frequencies rather than as a single one. We found the same effect in the Fourier spectrum of the combined LC.

In Fig. 3, we can see that several groups of frequencies appear in each run in the Fourier spectra, separated by almost the same frequency intervals (around 530 μHz). Some frequencies change their location in the Fourier spectrum from run to run, and in Fig. 3 (bottom panel) these appear as clusters of bars. The most commonly (more than 75 per cent of the runs) observed frequencies (and their range of amplitudes) from run to run were 1023.6 μHz (10–43 mma), 1623.6 μHz (26–41 mma), 2071.98 μHz (7–19 mma), 2536.8 μHz (5–11 mma) and 2658.8 μHz (5–18 mma). Less frequent (more than 40 per cent and less than 75 per cent of runs) but still significant frequencies (and their range of detected amplitudes) include 573.6 μHz (3.5–13 mma), 1158.8 μHz (6–20 mma), 2208.8 μHz (3.5–10 mma), 3093.9 μHz (3.5–9 mma) and 3243.9 μHz (3.5–10 mma).

The same frequencies were detected in the Fourier spectrum of the combined LC. The arrows in Fig. 4 mark the frequencies that were present most often. Frequencies with amplitudes close to the detection limit were observed less often. This means that during some runs, when the amplitudes fall below the detection limit, they were undetectable. Variations with small amplitudes were more common at higher frequencies, and these fall below the detection limit more often than lower frequency signals which had larger amplitudes. The higher frequency signals were seldom detectable in our data.

4 ANALYSIS OF THE COMBINED LIGHT CURVE AND ITS FOURIER SPECTRUM

Fig. 4 is a schematic comparison of frequencies detected in the combined data set (upper panel), with the total detected from individual runs. We see that some frequencies were not detected in the combined data set, because they had small amplitudes (often below the detection limit) for the majority of the runs, and consequently disappeared in the resultant Fourier spectrum, or because they were unstable and changed in amplitude from run to run.

Many signals in our 2004 data have not been detected in the previous years. This may be because some frequencies were unstable or their intrinsic amplitudes were variable with time. On the other hand, this could be caused by unresolved frequencies in the previous data sets. Closely spaced, unresolved frequencies produce an interference pattern, which at interferential maximum generated a signal of high amplitude and at the interferential minimum can make a frequency undetectable. To resolve such closely spaced frequencies, high temporal resolution (i.e. long-duration) data sets are required. The complete Fourier spectrum of PG 2303+243 pulsations calculated according to observations in 2004 and spectral window of observed combined LC are shown in Figs 5 and 6, respectively. As our 2004 data are the longest duration set obtained so far, these are the most helpful resolving closely spaced frequencies, albeit we cannot say whether some closely spaced peaks in Fourier spectrum are truly one of temporal resolution or such structures appear because of the strong variability of the modes' amplitudes. Long-duration data sets also offer the possibility of breaking them into shorter subsets to detect signals which appear transient because their amplitudes are small and variable.

From Fig. 3 we find that the shortest period is between 206 and 218 s (the mean value is 211 s). This period interval has positive detections in four runs while peaks were observed in at least six other runs, but below the detection limit and so are neither shown in the graph nor listed in the tables as detections. The same period was detected in the combined LC (211.28 s or 4733 μHz with an amplitude of 2.1 mma) and represents the shortest period in PG 2303+243. The next shortest period could be 233–234 s which was detected in seven of our runs and in the combined data set (234.1 s or 4272 μHz with an amplitude of 4.4 mma).

4.1 Groups of observed peaks

In Table 4, we provide all the frequencies, amplitudes and phases of the observed periodicities in PG 2303+243 during 2004 together with their uncertainties and detection limits. We noted groups of two and three peaks separated by 100–140 μHz (Table 3), but these are not equally spaced in periods.

The sequence of the groups is the following. The centre of the first group of three peaks is around 578 μHz in the Fourier spectrum, and two peaks are around 1092 μHz. Another group of three peaks appears around 1622 μHz, and again two peaks are around 2136 μHz. The next group consists of three peaks around 2650 μHz, two peaks follow near 3172 μHz, a group of three peaks is found around 3694 μHz and so on. The spacings between the central frequencies of adjacent groups of three peaks are about the same as the spacings between adjacent groups of two peaks, and are 1030–1040 μHz. The frequency differences between the groups of three peaks and the neighbouring groups of two peaks (spaces between neighbouring side peaks of two groups) are between 310 and 360 μHz. Not all groups of peaks have all their members detected as

Table 3. Summary of spacings between significant peaks. Numbers in parentheses corresponds to bumps below the detection limit.

Groups of frequencies	$f_{\rm range}$ [a] (μHz)	δf [b] (μHz)	$\Delta f_{\rm cont}$ [c] (μHz)
1st (3 freq)	447.5–578.6–(∼700)	131.1; (∼121)	–
2nd (2 freq)	1027.5–1157.7	130.2	327.5
3rd (3 freq)	1524.5–1622.3–1729.8	97.8; 107.5	366.8
4th (2 freq)	2071.8–2201.7	129.9	342.0
5th (3 freq)	2535.8–2650.3–2779.4	114.5; 129.1	334.1
6th (2 freq)	3100.9–3244.6	143.7	321.5
7th (3 freq)	3563.2–3693.9–3819.3	130.7; 125.4	330.7
8th (2 freq)	(∼4150)–4271.9	(∼122)	(∼343)
9th (3 freq)	(∼4580)–4733.2–4851.7	(∼153); 118.5	(∼308)
	(∼5200)–(–)		(∼348)

[a] Frequencies of peaks from single group.
[b] Spacing between frequencies in the group.
[c] Spacing between contiguous groups of frequencies.

Table 4. Multifrequency solution of the LC of PG 2303+243 obtained during the mini-campaign of 2004 September 5–20. The first column provides IDs for the detected frequencies. The numbers written in brackets in the last column show the difference between the observed frequencies (column 3) and the predicted combination of frequencies. The amplitude uncertainty is 0.21 mma and the resolution of the Fourier spectrum is 0.76 μHz.

ID	Comments[a]	Frequency (μHz)	$\sigma_{\rm freq}$	Amplitude (mma)	$\sigma_{\rm amp}$	Phase	$\sigma_{\rm phase}$	$A_{\rm min}$ [b] (mma)	Combinations of frequencies
f1	b	447.5	0.13	3.3	0.60	0.164	0.019	2.1	
f2		488.6	0.05	3.1	0.29	0.538	0.016	2.1	
f3	b,*,h1/2	578.6	0.11	6.2	0.60	0.306	0.009	2.1	(1/2) × f10 (0.3)
f4		594.5	0.07	2.2	0.30	0.196	0.030	2.1	
f5		938.0	0.07	2.2	0.29	0.316	0.025	2.0	
f6	b	1027.5	0.12	22.2	2.14	0.984	0.003	2.0	
f7	b,**,h0	1035.9	0.14	19.7	1.13	0.925	0.003	2.0	
f8		1044.3	0.05	3.9	0.35	0.662	0.011	2.0	
f9		1145.2	0.05	3.9	0.31	0.487	0.012	2.0	
f10	**,h0	1157.7	0.02	7.4	0.31	0.066	0.007	2.0	
f11		1165.8	0.03	4.9	0.30	0.276	0.012	2.0	
f12	b	1173.3	0.07	6.1	0.61	0.477	0.013	2.0	
f13		1287.7	0.06	2.5	0.29	0.619	0.020	2.0	
f14		1405.5	0.07	2.0	0.29	0.256	0.025	2.0	
f15		1489.0	0.07	2.2	0.30	0.424	0.024	2.0	
f16		1524.5	0.06	2.7	0.31	0.668	0.020	2.0	
f17		1527.7	0.06	2.5	0.31	0.737	0.019	2.0	
f18		1606.2	0.03	4.9	0.29	0.119	0.010	2.0	f3+f6 (0.1)
f19	*,h0	1622.3	0.00	31.3	0.29	0.055	0.002	2.0	
f20	***	1729.8	0.05	2.8	0.29	0.815	0.018	1.9	
f21	b,**,h1	2071.8	0.08	9.4	0.59	0.158	0.005	1.9	2 × f7 (0.0)
f22	**	2201.7	0.04	3.4	0.30	0.167	0.015	1.9	f3+f19 (0.8)
f23		2211.6	0.07	2.2	0.30	0.398	0.023	1.9	
f24	***	2535.8	0.02	7.3	0.31	0.300	0.010	1.9	
f25	b	2559.5	0.16	2.8	0.61	0.084	0.025	1.8	
f26	b,*	2650.3	0.24	10.0	1.38	0.305	0.006	1.8	f6+f19 (0.5)
f27		2658.1	0.04	4.5	0.31	0.348	0.011	1.8	f7+f19 (0.1)
f28	b,***	2779.4	0.14	3.6	0.60	0.290	0.014	1.8	f10+f19 (0.6)
f29	b,**	3100.9	0.14	3.1	0.60	0.030	0.017	1.8	
f30	h2	3107.4	0.06	2.4	0.30	0.221	0.021	1.8	3 × f7 (0.3)
f31	**,h1	3244.6	0.03	5.2	0.30	0.479	0.010	1.8	2 × f19 (0.0)
f32	b	3563.2	0.20	2.6	0.63	0.388	0.020	1.7	f6+f24 (0.1)
f33	*	3693.9	0.04	3.3	0.29	0.383	0.015	1.7	f19+2 × f7 (0.2)
f34		3819.3	0.09	2.3	0.30	0.962	0.022	1.7	
f35		3823.9	0.08	1.9	0.30	0.881	0.027	1.7	f11+f7+f19 (0.1)
f36	b,**	4271.9	0.14	3.2	0.60	0.840	0.029	1.6	
f37		4733.2	0.08	2.1	0.31	0.211	0.030	1.6	
f38	b,***	4851.7	0.19	2.3	0.60	0.164	0.019	1.6	

[a] b – averaged frequency, calculated for peaks broadened due to variable amplitude; * – central frequency in a group of three frequencies; ** – one of the frequencies in a group of two (see text); *** – outer frequency in a group of three; h1/2 – subharmonic (1/2 × h0); h0 – fundamental frequency; h1 – first harmonic (2 × h0); h2 – second harmonic (3 × h0).

[b] $A_{\rm min}$ – detection limit for each frequency.

some were below the detection limit in the noise. The frequencies that belong to groups are marked in Table 4 by ** for groups of two peaks, * for the central peak of groups of three peaks and *** for marginal peaks of groups of three. In Fig. 5, we see bumps of 1.5 and 1.3 mma around 4150, 4580 and 5200 μHz which could be the lowest frequency members of some groups of two or three peaks. These frequencies are not in our list of determined frequencies, because their amplitudes were smaller than the detection limit and cannot be trusted. However, if intrinsic, they would complete the multiplets.

4.2 Observed broadened peaks

The fitted frequencies above the detection limit, their amplitudes with 1σ errors, the detection limit $A_{\rm min}$ for each frequency and possible combinations of frequencies are shown in Table 4. The uncertainties given in Table 4 were calculated using PERIOD04. The amplitude uncertainty (0.21 mma) shows a mismatch of observed and calculated LCs. The $\sigma_{\rm amp}$ values (sixth column) are calculated using a least-squares fit in PERIOD04. It gives an uncertainty for every separate estimated signal. If the amplitude is variable, its $\sigma_{\rm amp}$ is larger, and if the amplitude is stable, its $\sigma_{\rm amp}$ is smaller.

Since some amplitudes varied over short time-scales (sometimes comparable to individual run lengths) the width of such peaks in the Fourier spectra can be larger than the frequency resolution calculated from the length of the run, and PERIOD04 may find more than one (nearby) frequency. Such frequencies are marked with a 'b' in Table 4, which means they possess broadened peaks due to variable amplitude. We prefer this interpretation over two to three

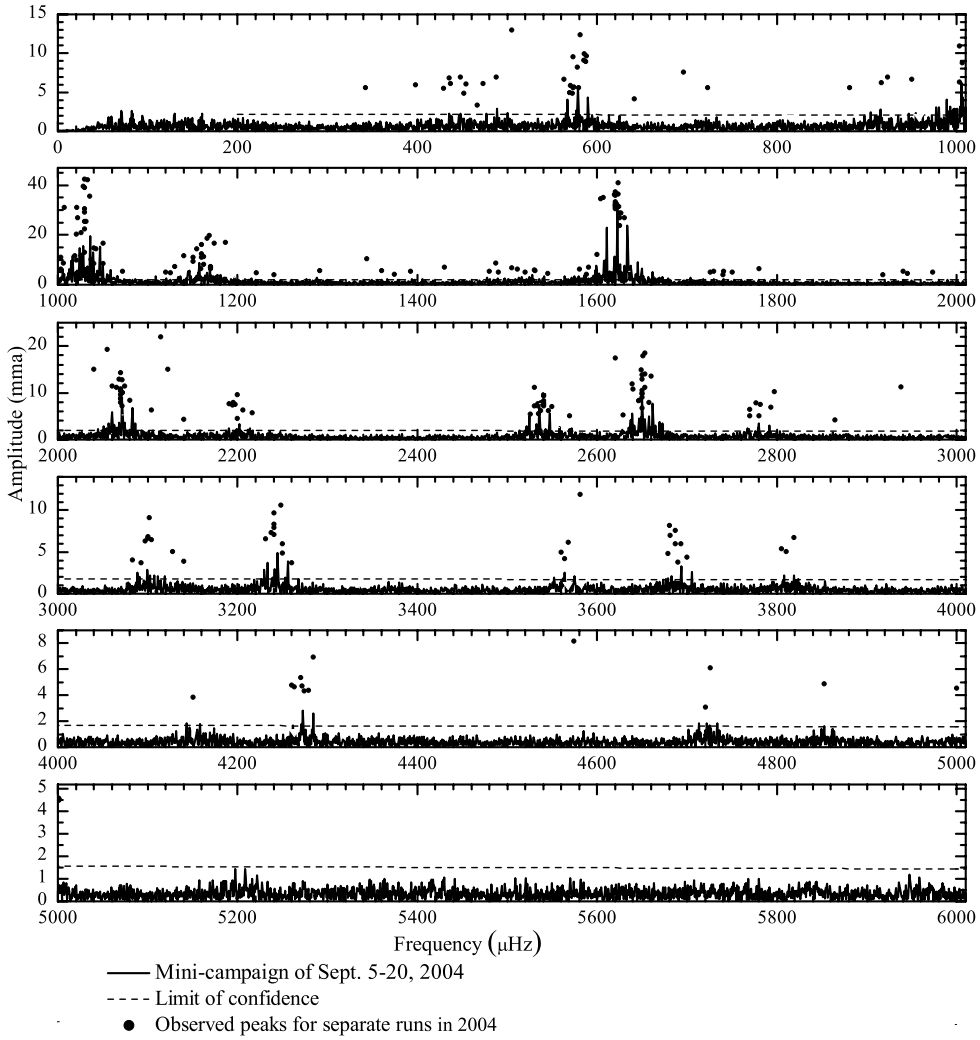

Figure 5. Comparison of the Fourier spectrum of the combined LC of PG 2303+243 observed during the mini-campaign of 2004 September 5–20 (solid curve), with detected frequencies and amplitudes for each separate run (dots). The dashed line corresponds to the frequency-dependent detection limit, when FAP = 0.001.

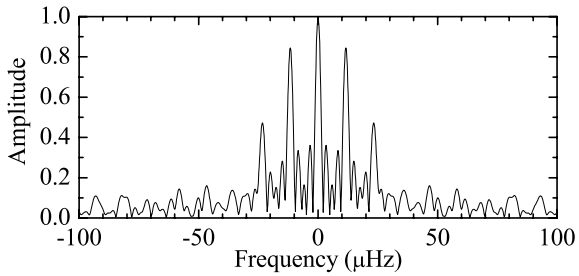

Figure 6. The spectral window of the combined LC during the mini-campaign of 2004 September 5–20.

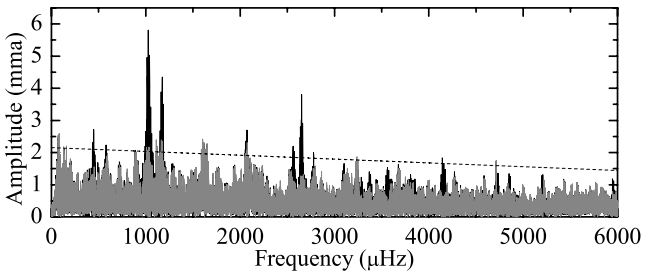

Figure 7. The Fourier spectrum of the residuals after pre-whitening. Black curve: only frequencies listed in Table 4 were used for pre-whitening. Grey curve: all fitted frequencies (before averaging broadened peaks) were used for pre-whitening. The dotted line shows the detection limit of the total data set for FAP = 0.001.

unresolved peaks separated by less than 3 μHz. Later, these possible unresolved frequencies were amplitude weighted and averaged.

For frequency and amplitude evaluation, the Levenberg–Marquardt non-linear least-squares fitting procedure in PERIOD04 was used. As a by-product of the least-squares fits, an error matrix is available and used for the calculation of a parameter's uncertainty. The least-squares fits to the data (Table 4) gave residuals (χ) of 28 mma and an amplitude uncertainty of 0.21 mma. The amplitude uncertainty shows a mismatch of observed and calculated LCs. The Fourier spectra of the averaged and non-averaged pre-whitening residuals used for this procedure are shown in Fig. 7. As previously stated, the averaged frequencies calculated for broadened peaks are marked with a 'b' in Table 4. In the Fourier spectra of the pre-whitening residuals, several quite high peaks appear at those

frequencies. They cannot be removed completely using PERIOD04 with the same width for all peaks.

4.3 Combinations of frequencies

We searched Table 4 for combination frequencies. Three frequencies generate harmonics: f7, f10 and f19. It is possible that f10 has a subharmonic at f3, because the amplitude of f10 is slightly larger than the amplitude of f3. Conversely, f3 may be an independent frequency which produces a first harmonic at f10, or both could be independent frequencies, and only coincidentally appear to be harmonics. It is not possible to distinguish between these three scenarios, though we favour the interpretation that f3 is the subharmonic of f10. We note in addition that a third harmonic of f7 may exist at 4142.8 μHz, but it is below the detection limit.

The combination frequencies were identified under the assumption that signals with amplitudes smaller than 4 mma cannot be parent frequencies, and that parent frequencies should have larger amplitudes than the combination frequency. The same is valid even when amplitudes vary over time, because the amplitude changes of the parent signals and the combination frequency are correlated. We also required that the difference between the predicted combination frequency and the observed value cannot be larger than 0.8 μHz, i.e. larger than the rounded resolution (0.76 μHz) of the data set. In addition, we assume that combination frequencies cannot produce other combination frequencies, but harmonics of higher order can be a part of the combination. All combinations are shown in the last column of Table 4. The numbers in parentheses indicate the difference between the calculated combination and the observed frequency.

4.4 Observed multiplets

Among the detected frequencies, we found an obvious triplet consisting of 1027.5, 1035.9 and 1044.3 μHz, with m equal to -1, 0 and $+1$, respectively (assuming a $l = 1$ mode), and differences between contiguous frequencies of 8.4 μHz. It is also likely that the peaks at 578.6 and 594.5 μHz are a part of another triplet and their m values are -1 and $+1$, respectively. These two peaks should have a central peak ($m = 0$) around 586.5 μHz, for almost the same spacing of 8.0 μHz as the other triplet around 1035.8 μHz, but a central peak is not observed in this case.

WDs are slow rotators. The shortest rotation period of a ZZ Ceti star is 9 h for G 226−29 (Kepler et al. 2005a) and the longest rotation period is 55 h for GD 154 (Pfeiffer et al. 1996). According to Ledoux & Walraven (1958) or Winget et al. (1991), $P_{\rm rot} = \{1 - [l(l+1)]^{-1}\}/\delta f_l$ for g modes in the asymptotic limit. If we assume $\delta f_l = 8.4$ μHz and $l = 1$, the rotation period of PG 2303+243 is 0.69 d or 16.5 h.

4.5 Independent frequencies

For further analysis we need to identify the independent frequencies (Table 5) out of the values listed in Table 4. Combinations of frequencies and split frequencies can only mislead the asteroseismic interpretation of our measurements. We have excluded all combinations generated by two frequencies from Table 4, together with the first and second harmonics and frequencies of multiplets with $m \neq 0$.

Further inclusions in Table 5 were made for frequencies f3 and f10 because it is difficult to determine which of them is the fundamental frequency h0, and which of them is the harmonic of the fundamental frequency. They are potentially both independent frequencies, and only coincidentally appear to be harmonics.

Table 5. The list of possible independent frequencies of PG 2303+243, observed during the mini-campaign of 2004 September.

No.	Frequency (μHz)	Period (s)	Amplitude (mma)	Phase
1	447.5	2234.6	3.3	0.164
2	488.6	2046.7	3.1	0.538
3	586.5	1705.0	1.6	0.869
4	938.0	1066.1	2.2	0.316
5	1035.9	965.3	19.7	0.925
6	1145.2	873.2	3.9	0.487
7	1157.7	863.8	7.4	0.066
8	1165.8	857.8	4.9	0.276
9	1173.3	852.3	6.1	0.477
10	1287.7	776.6	2.5	0.619
11	1405.5	711.5	2.0	0.256
12	1489.0	671.6	2.2	0.424
13	1524.5	656.0	2.7	0.668
14	1527.7	654.6	2.5	0.737
15	1622.3	616.4	31.3	0.055
16	1729.8	578.1	2.8	0.815
17	2211.6	452.2	2.2	0.398
18	2535.8	394.4	7.3	0.300
19	2559.5	390.7	2.8	0.084
20	3100.9	322.5	3.1	0.030
21	3819.3	261.8	2.3	0.962
22	4271.9	234.1	3.2	0.840
23	4733.2	211.3	2.1	0.211
24	4851.7	206.1	2.3	0.164

Consequently, the final list of independent frequencies contains the 24 signals listed in Table 5. However, some of these could still be parts of multiplets, for example 1165.8 μHz ($m = 0$ or -1) and 1173.3 μHz ($m = +1$ or 0) with a spacing of 7.5 μHz; 2535.8 μHz ($m = -2$ or -1) and 2559.5 μHz ($m = +1$ or $+2$) with a spacing of 7.9 μHz.

If our criterion for the detection limit would be more relaxed (e.g. FAP = 0.01), then peaks with low amplitudes at 4713.3 μHz ($m = -1$) and 4733.2 μHz ($m = +1$) may also belong to a triplet with a spacing of 9.95 μHz. The same is valid for other peaks with low amplitudes at 2196.1 μHz ($m = -1$) and 2211.6 μHz ($m = 1$) with a spacing of 7.5 μHz. However, none of these frequency pairs forms obvious multiplets. In most cases, there is no central peak of $m = 0$ and the spacing is not uniform, varying between 7.5 and 9.95 μHz. All these signals are therefore included in our list as independent frequencies.

5 CONCLUSIONS

The high amplitude and large number of frequencies in the pulsation spectrum of PG 2303+243 make it a good candidate for an asteroseismic study. Since the star had not been observed since 1992, and its pulsation spectrum changes from run to run, we organized a mini-campaign at six observatories during 2004 September with the goal to resolve the star's pulsation spectrum. We also expected more than 22 periods to be present.

During the 15-d mini-campaign, nearly 137 h and 20 500 points of photometric time series data were obtained with a combined duty cycle of 35.2 per cent. We found that some frequencies from previous observations were not detectable in 2004 and some

pulsations observed in 2004 were not previously detected. This can be explained by a long-term amplitude variability. When the amplitudes become smaller than the detection limit, we cannot detect them.

We also found that some amplitudes vary dramatically from run to run. The resultant peaks in the Fourier spectra are broader than expected from the resolution of the data set. PERIOD04 then detects two to three frequencies instead of one, spaced by 3 μHz (in our case). These closely spaced frequencies were amplitude weighted, averaged and examined with the result that we classify these as 'broadened'. The reason for broadening may be close harmonic modes n, as specified in models, and/or a combination of runs with different sensitivity (noise caused by some combination of weather, moon light and various-sized telescopes and detecting equipment).

All 38 frequencies, amplitudes and phases are listed in Table 4 together with the errors in all parameters. According to this list, we found three fundamental frequencies, which generated two first harmonics, one second harmonic and one subharmonic, together with nine possible combinations of frequencies. We discovered one obvious triplet at 1027.5, 1035.9 and 1044.3 μHz with spacings of 8.4 μHz. The rotation period of PG 2303+243, when $\delta f_l = 8.4$ μHz and $l = 1$, is 0.69 d or 16.5 h.

After removing the first and second harmonics, combination frequencies and rotationally split triplet components from Table 4, we established a list of 24 possible independent frequencies. This list will be used for further investigations of PG 2303+243 with the analysis of pulsations. The results will be presented in a subsequent paper.

ACKNOWLEDGMENTS

We thank Gerard Vauclair, Noel Dolez and Gražina Tautvaišienė for a critical reading of the manuscript and for helpful suggestions. We are grateful to the referee S. O. Kepler for a number of helpful suggestions for improvement in the paper.

REFERENCES

Althaus L. G., Córsico A. H., Isern J., Garcia-Berro E., 2010, A&AR, 18, 471
Bergeron P., Wesemael F., Lamontagne R., Fontaine G., Saffer R. A., Allard N. F., 1995, ApJ, 449, 258
Bergeron P., Fontaine G., Billeres M., Boudreault S., Green E. M., 2004, ApJ, 600, 404
Bischoff-Kim A., Montgomery M. H., Winget D. E., 2008a, ApJ, 675, 1505
Bischoff-Kim A., Montgomery M. H., Winget D. E., 2008b, ApJ, 675, 1512
Bradley P. A., 1998, Baltic Astron., 7, 111
Bradley P. A., 2001, ApJ, 552, 1
Brassard P., Fontaine G., Wesemael F., Hansen C. J., 1992, ApJS, 80, 369
Brickhill A. J., 1983, MNRAS, 204, 537
Brickhill A. J., 1992, MNRAS, 259, 519
Castanheira B. G., Kepler S. O., 2008, MNRAS, 385, 430
Castanheira B. G., Kepler S. O., 2009, MNRAS, 396, 1709
Castanheira B. G. et al., 2007, A&A, 462, 989
Castanheira B. G., Kepler S. O., Kleinman S. J., Nitta A., Fraga L., 2010, in Werner K., Rauch T., eds, AIP Conf. Proc. Vol. 1273, 17th European White Dwarf Workshop. Am. Inst. Phys., New York, p. 500
Clemens J. C., 1993, Baltic Astron., 2, 407
Córsico A. H., Benvenuto O. G., Althaus L. G., Isern J., Garcia-Berro E., 2001, New Astron., 6, 197
De Gennaro S., von Hippel T., Winget D. E., Kepler S. O., Nitta A., Koester D., Althaus L., 2008, AJ, 135, 1
Dolez N., Vauclair G., 1981, A&A, 102, 375
Dolez N. et al., 2006, A&A, 446, 237
Fleming T. A., Liebert J., Green R. F., 1986, ApJ, 308, 176
Fontaine G., Brassard P., 2008, PASP, 120, 1043
Fontaine G., Brassard P., Bergeron P., 2001, PASP, 113, 409
Gianninas A., Bergeron P., Fontaine G., 2005, ApJ, 631, 1100
Gianninas A., Bergeron P., Fontaine G., 2006, AJ, 132, 831
Handler G., Romero-Colmenero E., Montgomery M. H., 2002, MNRAS, 335, 399
Kanaan A., Kepler S. O., Giovannini O., Winget D. E., Montgomery M., Nitta A., 1998, Baltic Astron., 7, 183
Kepler S. O., 1993, Baltic Astron., 2, 515
Kepler S. O. et al., 1995, Baltic Astron., 4, 221
Kepler S. O., Castanheira B. G., Saraiva M. F. O., Nitta A., Kleinman S. J., Mullally F., Winget D. E., Eisenstein D. J., 2005a, A&A, 442, 629
Kepler S. O. et al., 2005b, ApJ, 634, 1311
Kepler S. O., Castanheira B. G., Costa A. F. M., Koester D., 2006, MNRAS, 372, 1799
Kleinman S. J. et al., 2004, ApJ, 607, 426
Koester D., Allard N. F., 2000, Baltic Astron., 9, 119
Koester D., Holberg J. B., 2001, in Provencal J. L., Shipman H. L., MacDonald J., Goodchild S., eds, ASP Conf. Ser. Vol. 226, 12th European Workshop on White Dwarfs. Astron. Soc. Pac., San Francisco, p. 299
Koester D., Vauclair G., 1997, in Isern J., Hernanz M., Garcia-Berro E., eds, White Dwarfs. Kluwer, Dordrecht, p. 429
Koester D., Kepler S. O., Kleinman S. J., Nitta A., 2009, J. Phys. Conf. Ser., 172, 012006
Ledoux P., Walraven Th., 1958, in Flügge S., ed., Handbuch der Physik, Vol. 51. Springer-Verlag, Berlin, p. 353
Lenz P., Breger M., 2005, Communications Asteroseismology, 146, 53
McGraw J. T., Fontaine G., Lacombe P., Dearborn D. S. P., Gustafson J., Starrfield S. G., 1981, ApJ, 250, 349
Montgomery M. H., 2005a, ApJ, 633, 1142
Montgomery M. H., 2005b, in Koester D., Moehler S., eds, ASP Conf. Ser. Vol. 334, 14th European Workshop on White Dwarfs. Astron. Soc. Pac., San Francisco, p. 553
Montgomery M. H., 2007, in Napiwotzki R., Burleigh M. R., eds, ASP Conf. Ser. Vol. 372, 15th European Workshop on White Dwarfs. Astron. Soc. Pac., San Francisco, p. 635
Montgomery M. H., Williams K. A., Winget D. E., Dufour P., De Gennaro S., Liebert J., 2008, ApJ, 678, L51
Mukadam A. S., Winget D. E., von Hippel T., Montgomery M. H., Kepler S. O., Costa A. F. M., 2004, ApJ, 612, 1052
Mukadam A. S., Montgomery M. H., Winget D. E., Kepler S. O., Clemens J. C., 2006, ApJ, 640, 956
Nather R. E., Winget D. E., Clemens J. C., Hansen C. J., Hine B. P., 1990, ApJ, 361, 309
Pech D., Vauclair G., Dolez N., 2006, A&A, 446, 223
Pfeiffer B. et al., 1996, A&A, 314, 182
Riddle R. L., 2003, Baltic Astron., 12, 183
Robinson E. L., 1980, in Hill H. A., Dziembowski W. A., eds, Lecture Notes in Physics, Vol. 125, Nonradial and Nonlinear Stellar Pulsation. Springer-Verlag, Berlin, p. 444
Scargle J. D., 1982, ApJ, 263, 835
Szkody P. et al., 2010, ApJ, 710, 64
Tremblay P.-E., Bergeron P., 2009, ApJ, 696, 1755
Vauclair G., Dolez N., Chevreton M., 1987, A&A, 175, L13
Vauclair G. et al., 1992, A&A, 264, 547
Vuille F., Brassard P., 2000, MNRAS, 313, 185
Weidemann V., 2000, A&A, 363, 647
Winget D. E., 1988, in Christensen-Dalsgaard E. J., Frandsen S., eds, Proc. IAU Symp. 123, Advances in Helio- and Asteroseismology. Reidel, Dordrecht, p. 305
Winget D. E., Fontaine G., 1982, in Cox J. P., Hansen C. J., eds, Pulsations in Classical and Cataclysmic Variable Stars. Univ. Kolorado Press, Boulder, CO, p. 46
Winget D. E., Kepler S. O., 2008, ARA&A, 46, 157
Winget D. E., van Horn H. M., Tassoul M., Fontaine G., Hansen C. J., Carroll B. W., 1982, ApJ, 252, 65

Winget D. E., Hansen C. J., Liebert J., van Horn H. M., Fontaine G., Nather R. E., Kepler S. O., Lamb D. Q., 1987, ApJ, 315, 77
Winget D. E. et al., 1991, ApJ, 378, 326
Wu Y., 2001, MNRAS, 323, 248
Wu Y., Goldreich P., 2001, ApJ, 546, 469
Yeates C. M., Clemens J. Ch., Thompson S. E., Mullally F., 2005, ApJ, 635, 1239

This paper has been typeset from a TEX/LATEX file prepared by the author.